PHYSICS

Pseudo-spin switches and Aharonov-Bohm effect for topological boundary modes

Yuma Kawaguchi[1]†, Daria Smirnova[2]†, Filipp Komissarenko[1], Svetlana Kiriushechkina[1], Anton Vakulenko[1], Mengyao Li[3], Andrea Alù[1,4,5], Alexander B. Khanikaev[1,5,6]*

Topological boundary modes in electronic and classical-wave systems exhibit fascinating properties. In photonics, topological nature of boundary modes can make them robust and endows them with an additional internal structure—pseudo-spins. Here, we introduce heterogeneous boundary modes, which are based on mixing two of the most widely used topological photonics platforms—the pseudo-spin–Hall-like and valley-Hall photonic topological insulators. We predict and confirm experimentally that transformation between the two, realized by altering the lattice geometry, enables a continuum of boundary states carrying both pseudo-spin and valley degrees of freedom (DoFs). When applied adiabatically, this leads to conversion between pseudo-spin and valley polarization. We show that such evolution gives rise to a geometrical phase associated with the synthetic gauge fields, which is confirmed via an Aharonov-Bohm type experiment on a silicon chip. Our results unveil a versatile approach to manipulating properties of topological photonic states and envision topological photonics as a powerful platform for devices based on synthetic DoFs.

INTRODUCTION

Topological phases in quantum materials and various wave systems—electronic (*1*, *2*), acoustic (*3*, *4*), mechanical (*5*), and photonics (*6*–*8*)—are characterized by nontrivial band connectivity in momentum space, giving rise to topological boundary modes endowed with some fascinating properties (*9*–*12*). Thus, in systems with broken time-reversal (TR) symmetries, such as quantum Hall and Haldane topological phases, one attains unidirectional transport with unprecedented robustness to defects and disorder. Unfortunately, breaking TR symmetry to attain such topological phases (*9*, *10*) is notoriously challenging at optical frequencies. Hence, an alternative, symmetry-based approach has been especially fruitful in photonics (*7*). The latter enables a class of symmetry-protected topological systems governed by symmetries through which modes are endowed with spectral degeneracies that play a role of synthetic degrees of freedom (DoFs), referred to as pseudo-spins (*13*, *14*) and valley (*15*–*17*) DoFs. While offering the robustness that is limited (*18*) to a set of symmetry-preserving defects, these systems still exhibit unidirectional boundary modes, with modes of opposite pseudo-spins propagating in opposite directions.

Besides the early interest in symmetry-protected topological systems as a tabletop platform to emulate fundamental topological phenomena, more recently focus has shifted to more applied aspect, including for optical field trapping for lasing (*19*–*23*), nonlinear effects (*24*–*26*), and light-matter interactions (*27*–*31*). Topological photonic boundary modes have been also explored in the context of quantum applications (*32*–*36*). However, the concept of pseudo-spin in light-matter interactions and quantum applications remains largely unexplored. It only recently became clear that pseudo-spin can be used to tune radiative leakage of modes and strength of the light-matter coupling in topological metasurfaces (*37*). However, even more exciting prospects can arise in quantum optics by using symmetry engineered photonic pseudo-spinors as qubits for encoding quantum information. While the polarization DoF of light has been widely leveraged in quantum research in free-space experimental settings (e.g., polarization-entangled photons and polarization-squeezed states of light), it was not the case for integrated photonic platforms where other types of quantum entanglement are used (*38*). The reason is obviously related to the collapse of the polarization degeneracy that produces generally nondegenerate TE and TM modes. In this regard, the synthetic pseudo-spins may offer an excellent alternative to free-space polarization on chip and exploited along with other unique features of topological boundary modes stemming from their spin-polarized character for quantum applications.

In this work, we experimentally demonstrate the possibility of an ultimate control over multiple characteristics of boundary modes in topological photonic metasurfaces. By using the modern theory of polarization applied to photonics, we show that pseudo-spin can be continuously tuned by unitary transformations realized via adiabatic change in the metasurface geometry. Along with tuning the radiative properties of the boundary modes, this allows us to realize X-gate operation in the pseudo-spin space and to use the adiabatic pseudo-spin evolution to generate the geometrical phase.

RESULTS

Heterogeneous topological photonic insulators

The two approaches commonly used to attain topological features in photonic chips at optical frequencies are based on valley-Hall (VH) (*39*–*41*) and pseudo-spin–Hall (PSH) effects (*42*–*44*), which can be implemented in silicon-on-insulator structures (Fig. 1, C to G). The VH systems rely on the hexagonal symmetry of a graphene-like photonic lattice (*45*), whose sublattice symmetry is reduced via dimerization (Fig. 1E). In the VH picture, this symmetry reduction gives rise

[1]Department of Electrical Engineering, The City College of New York, New York, NY 10031, USA. [2]Research School of Physics, The Australian National University, Canberra, ACT 2601, Australia. [3]Institute of Materials Research, Tsinghua Shenzhen International Graduate School, Tsinghua University, Shenzhen 518055, China. [4]Photonics Initiative, Advanced Science Research Center, City University of New York, New York, NY 10031, USA. [5]Physics Program, Graduate Center of the City University of New York, New York, NY 10016, USA. [6]Department of Physics, The City College of New York, New York, NY 10031, USA.
*Corresponding author. Email: akhanikaev@ccny.cuny.edu
†These authors contributed equally to this work.

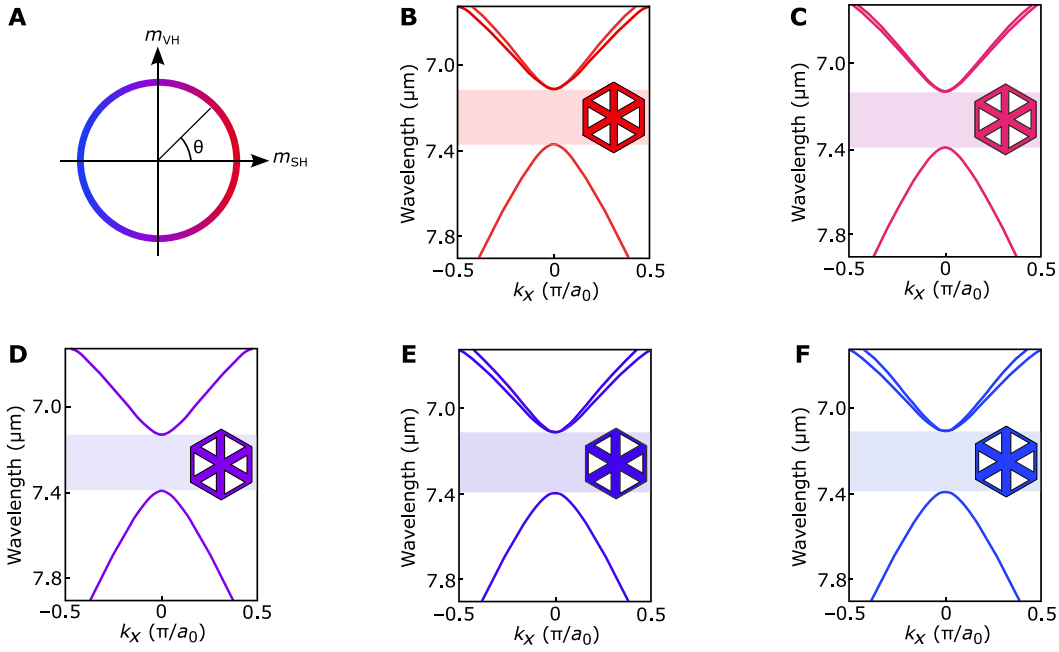

Fig. 1. Bulk states corresponding to spin, valley, and heterogeneous topological photonic insulators. (**A**) A rotation parameter θ in the spin-valley phase space. (**B** to **E**) Bulk bands around the Γ point with (B) θ = 0. (C) θ = π/4 . (D) θ = π/2. (E) θ = 3π/4. (F) θ = π.

to an effective gauge field acting differently on the bands at the two (K and K′) valleys in momentum space—associated with a binary synthetic valley DoF ($|v\rangle = |+\rangle$ or $|v\rangle = |-\rangle$).

To emulate the spin-Hall effect in photonics, one can rely on pseudo-TR symmetries, typically stemming from point symmetries of the photonic lattice. In the case of the Wu and Hu design (*14*), one considers a perturbed graphene lattice with C_6 symmetry such that its unit cell contains a hexamer of dielectric scatterers, which are either brought closer to the unit cell center (shrinking; Fig. 1C) or moved farther apart (expanding; Fig. 1G). Because the lattice has an exact symmetry at $k = 0$, the rotational symmetry generates a pseudo-spin $|s\rangle = |\uparrow, \downarrow\rangle$ (the orbital momentum of the modes) in the vicinity of the Γ-point (*46*). Similar to the VH case, the effect of the lattice perturbations can be treated as a synthetic gauge field acting on the pseudo-spin $|s\rangle$, inducing a transition between topological "expanded" and trivial "shrunken" structures.

Both VH and PSH-like systems are fundamentally based on the same lattice geometry, they exhibit total of four bands, and hence, their effective description of topological photonic systems can be done in the four-dimentional Hilbert space, for instance spanned by the two (pseudo-spin $|s\rangle$ and valley $|v\rangle$) synthetic DoFs, i.e., with the two sets of Pauli matrices ($\hat{s}$ and $\hat{\sigma}$, respectively) (*14*, *44*). The corresponding analytical formulation in terms of effective 4 × 4 Dirac-type Hamiltonians has been successfully adopted for both valley and pseudo-spin types in photonic (*47*, *48*) and mechanical systems (*49*, *50*). In photonics contexts, it was shown that one can implement additional control over photonic states, including for manipulation of bulk (*47*, *48*) and boundary (*51*) states, and more recently, for trapping light and lasing in 0D topological vortex cavities (*52*–*55*). An interesting approach to manipulate pseudo-spin was proposed (*49*), where adiabatic variation of Kekulé perturbations in micromechanical system was used to manipulate spin-Hall type boundary modes, including for flipping auxiliary orbital DoF, i.e., pseudo-spin.

Here, we propose to leverage such adiabatic variations in a heterogeneous topological photonic system with nontrivial VH and PSH phases, and we realize control over synthetic optical pseudo-spins, but we also show that distinct radiative properties of VH and PSH boundary modes enables fine-tuning of radiative coupling of the hybrid VH-PSH boundary modes. Moreover, the radiative nature of the modes allows us to realize unidirectional excitation of the boundary modes by circularly polarized far field and to perform a subsequent transformation of radiative PSH states into nonradiative VH modes via an adiabatic geometry variation. Thus, the possibility of having two types of gauge fields acting on different synthetic DoFs in the same structure opens exciting opportunities for manipulating topological photonic states.

Considering the photonic system in hands, we note that for truly distinct topological phases, the topological transition must be accompanied by a closing of the bandgap. It can be seen from Fig. 1 (C to G), however, that during the transformation of the unit cell geometry from PSH to VH type, the topological bandgap remains open, indicating that these two phases are particular cases of a more general crystalline insulator with bulk polarization. This is indeed confirmed by calculating the locations of the Wannier function in the tight binding model for various combinations of PSH and VH perturbations that keep the full-gap width constant (Supplementary Materials, section H). Thus, both systems can be understood in the context of "quantum chemistry", which allows to interpret boundary modes as the consequence of nonvanishing polarization of the bulk due to the displacement of a Wannier function within the unit cell (*56*–*59*) (Supplementary Materials, section H). Our calculations (Supplementary Materials, section H, and fig. S11) imply that the system has nonvanishing polarization for every angle of mass term except the trivial

pure PSH phase ($\theta = 0$). Around pure topological PSH phase ($\theta = \pi$), the C_6 lattice symmetry breaking induces a shift of the Wannier center within the unit cell from the edge into its volume. Then, the Wannier polarization evolves into the VH and then the trivial PSH phase continuously with the rotation of the mass angle θ. We thus deduce that, for a system with coexisting symmetry breaking mechanisms, i.e., dimerization for VH and shrink/expand for PSH, by varying two types of perturbations, the system undergoes a transition between the two seemingly distinct topological phases.

This unified description of the VH and PSH topological phases justifies their direct comparison with the VH structure with an enlarged unit cell as in Fig. 1. Such choice of the unit cell yields an artificial folding of the valleys of the original graphene lattice into the Γ-point of the reduced Brillouin zone, just like for PSH system. We note that because of the artificial nature of such folding, appearance of the folded bands above the light cone does not actually result in their radiative leakage.

Next, we leverage this connection between PSH and VH phases to gain functionalities. First, we adopt a continuous geometry transformation of the design in Fig. 1, which was optimized to maintain a nearly constant bandgap width between PSH and VH systems. Second, we adopt an effective Hamiltonian pseudo-spin/valley 4×4 matrix description, with $\hat{H}_{\mathrm{PSH}}$ and $\hat{H}_{\mathrm{VH}}$ corresponding to the "pure" PSH and VH phases. In the latter picture, the VH and PSH regimes are connected by a unitary "gauge" transformation, $\hat{H}_{\mathrm{VH}} = \hat{U}_{\frac{\pi}{2}} \hat{H}_{\mathrm{PSH}} \hat{U}_{-\frac{\pi}{2}}$ (see Supplementary Materials, section A, for the detailed description), where $\hat{U}_{\frac{\pi}{2}}$ is the matrix representation of the geometry transformation that performs a π/2 rotation in the spin-valley parameter space schematically depicted in Fig. 1A. The unitary transformation $\hat{U}(\theta)$, parametrized by $\theta \in [0,2\pi)$, and the geometric lattice perturbations associated with it establish an infinite number of "gauge-transformed" systems connected to the original PSH phase (Fig. 1A). In this picture, $\theta = 0$ and $\theta = \pi$ correspond to the two PSH phases with positive and negative effective PSH mass m_{SH}, which are commonly referred to as trivial and topological, respectively, while $\theta = \pm\frac{\pi}{2}$ correspond to the two distinct VH phases with positive and negative valley mass m_{VH}, respectively.

Continuum of heterogeneous spin-valley–polarized edge states

In accordance with the bulk-interface correspondence, interfacing topological systems with opposite spin-Chern numbers, i.e., located at the opposite ends of the circle in Fig. 1, $\theta = 0$ and π, yields pseudo-spin–polarized (helical) boundary states. Similarly, a domain wall of two VH crystals $\theta = \pm\frac{\pi}{2}$ on the vertical axis yields pseudo-spin–polarized boundary states. It can thus be inferred that the existence of boundary states is associated with a π variation of θ across the interface between two domains ($\Delta\theta = \pi$) [also see (*49*)], even when the system is not purely PSH or VH type. Our analytical calculations based on the effective Hamiltonian approach (Supplementary Materials, section A) confirm that any gauge transformation $\hat{U}(\theta)$ preserves boundary states. Our first-principles calculations further confirm that there always exist "topologically opposite" geometries (with $\Delta\theta = \pi$) so that edge states emerge and have minimal bandgap. [Note that an adiabatic transition from one topology to another yields an arbitrarily small gap between the two edge states, making them gapless in the limit of infinitely smooth transition between the two domains (*37*, *60*)].

Figure 2 shows examples of pure and mixed PSH and VH structures with a domain wall at the center, confirming the presence of edge states localized at the interfaces in each scenario. These photonic crystals with both PSH and VH perturbations thus can be seen as a heterogeneous topological platform that merges the two types of topological systems, which are often considered as distinct. The color coding in Fig. 2 also clearly shows strong dependence of the radiative

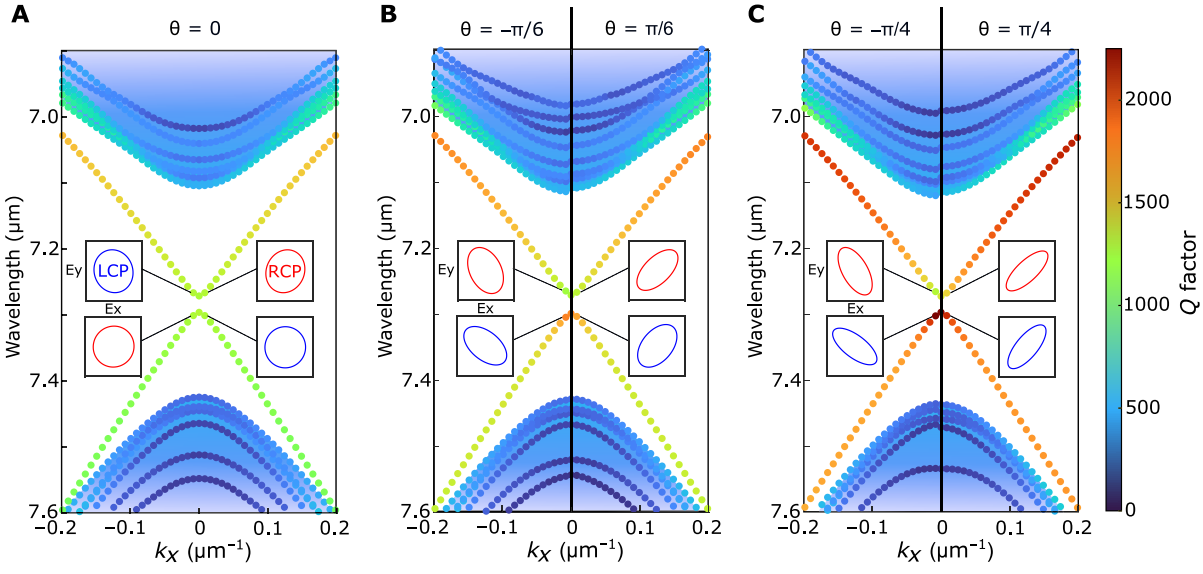

Fig. 2. Topological boundary modes for different values of PSH and VH perturbations. (**A**) Purely PSH boundary modes between two domains with $\theta = 0$ and $\theta' = \pi$. (**B**) Mixed PSH-VH boundary modes for $\theta = \pi/6$ and $\theta' = 7\pi/6$ (right side), $\theta = -\pi/6$ and $\theta' = 5\pi/6$ (left side). (**C**) Mixed PSH-VH boundary modes for $\theta = \pi/4$ and $\theta' = 5\pi/4$ (right side), $\theta = -\pi/4$ and $\theta' = 3\pi/4$ (left side). Insets: The far field polarization profiles for the boundary modes.

quality factor of the boundary modes depending on the value of angle θ, with the most radiative modes corresponding to the pure PSH boundary modes (θ = 0) with radiative quality factor $Q \approx 10^3$, and the least radiative (nonradiative, $Q \to \infty$) corresponding to the pure VH modes. For any value of θ, the presence of topological boundary modes is insured by a generalized bulk-boundary correspondence ($\Delta\theta = \pi$), and in general scenarios, the modes carry a combination of spin and valley polarizations intermixed with one another by means of the gauge transformation $\hat{U}(\theta)$ and have radiative quality factor withing the range of pure PSH and VH modes (i.e., from ~1000 to infinity). Thus, angle θ can be used for tuning radiative lifetime of the topological boundary states.

We experimentally tested heterogeneous modes in leaky metasurfaces with patterns shown in Fig. 1. The polarization state of far-field radiation for the PSH metasurface is known to be connected to the pseudo-spin of boundary states due to the angular momentum conservation—a feature that has been extensively used to selectively excite PSH-polarized edge modes and to confirm their unidirectional propagation. As shown in Fig. 2, the polarization state of the far-field radiation of the heterogeneous spin-valley–polarized modes also traces a well-defined pattern, with circularly polarized modes being the particular case for PSH edge modes. As we vary the mix between PSH and VH, the far-field polarization changes from circular to elliptical and becomes nearly linearly polarized at 45° with respect to the unit cell axes as the modes approach of the VH regime, at which point the modes become nonradiative.

To experimentally demonstrate these heterogeneous edge states and validate their properties, we experimentally fabricated several photonic crystals in silicon-on-sapphire substrates (shown in Fig. 3, A to C; see details on Materials and Methods). The samples were optimized to work in the mid-infrared range, and real-space and Fourier-plane (back focal plane) imaging was performed to visualize the edge modes and extract the edge spectra. In agreement with our theoretical predictions, the images in Fig. 3 confirm the localization and propagation of edge modes along the topological interfaces. Similar to pure PSH modes, the mixed edge modes are directionally excited with properly chosen handedness of the incident circularly polarized light, because of their elliptical polarization. However, the excitation of modes in both (forward and backward) directions becomes more and more visible (Fig. 3) for interfaces with increasing VH gauge field, because of increasing mismatch of the far fields of the modes with the circularly polarized optical excitation.

The experimental band structure (see Supplementary Materials, section G) confirms the nearly gapless character of the edge modes and shows that they span almost the entire topological bandgap. Being spin-valley polarized, the edge modes exhibit reflectionless propagation across lattice perturbations conforming to the lattice symmetry. For instance, similar to their pure PSH and VH cousins, the hybrid PSH and VH modes (for θ = 40°) can be routed around sharp bends of the domain wall (Supplementary Materials, section D).

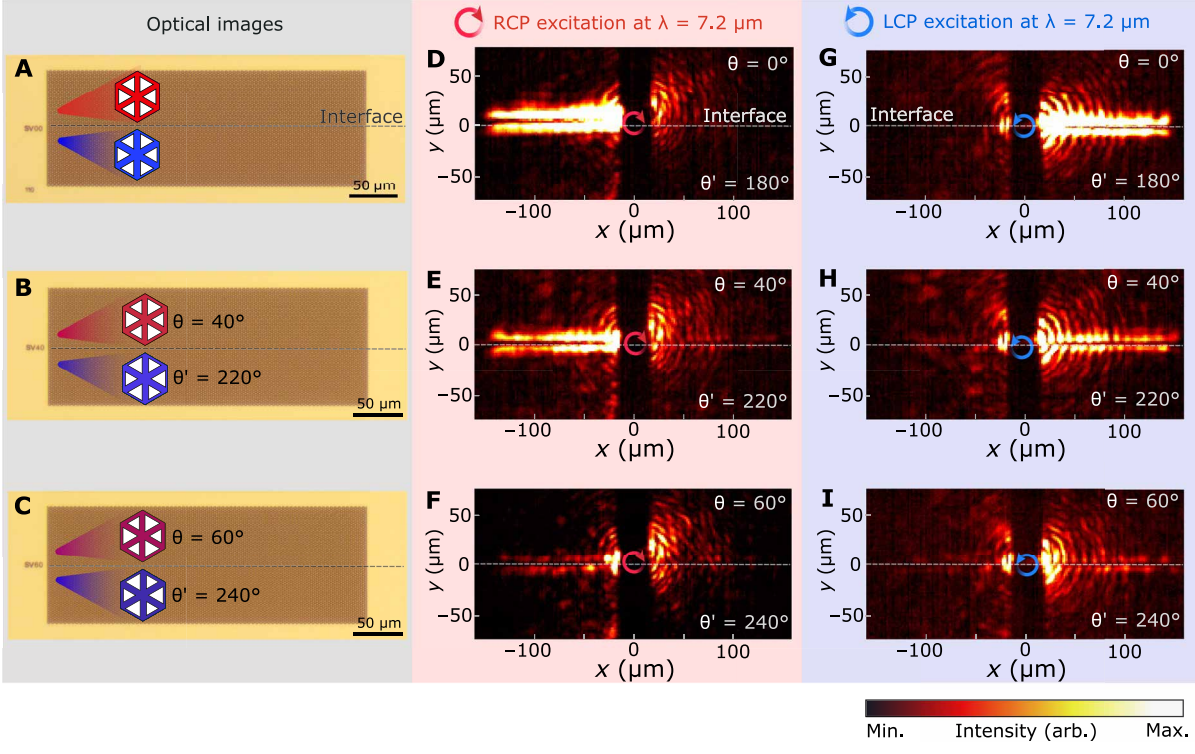

Fig. 3. PSH and VH (PSH-VH) heterogeneous topological boundary modes. (**A**, **D**, and **G**) θ = 0°, (**B**, **E**, and **H**) θ = 40°, and (**C**, **F**, and **I**) θ = 60°. (A) to (C) Optical images of the topological PSH and PSH-VH hybrid structures. (D) to (I) Real-space images of boundary modes propagating unidirectionally by right-handed circular polarized (RCP) [(D) to (F)] and left-handed circular polarized (LCP) [(G) to (I)] excitation around the mid-bandgap. The colored arrows in the real-space images present the position of excitation beam with the spot size ~20 μm at 7.2 μm and polarization (blue, LCP; red, RCP).

Topological one-way pseudo-spin switches

The possibility to engineer topological edge states with any fraction of pseudo-spin and valley DoF opens exciting opportunities to control and manipulate boundary modes. For pure VH and PSH designs, edge modes with either valley or pseudo-spin can propagate in a given direction, and there is no possibility to change or reverse it due to the pseudo-spin locking. The heterogeneous topological platform expands markedly the parameter space, implying that the pseudo-spin and valley DoFs can be transformed into one another. As the design of adjacent (topologically opposite) domains is slowly converted from PSH to VH (i.e., from $\theta = 0$ to $\theta = \frac{\pi}{2}$, with $\Delta\theta = \frac{\pi}{2}$), the pseudo-spin is expected to change into valley polarization. Moreover, the continuity of the parameter θ-circle allows us to flip (reverse) the valley polarization or the pseudo-spin by slowly changing θ by π along the interface, without reversing the propagation direction of the boundary mode. Thus, the heterogeneous topological interfaces enable the realization of arbitrary unidirectional switches for synthetic DoFs via unitary transformations, e.g., $|\psi_{edge}(\theta_0 + \delta\theta)\rangle = \hat{U}(\delta\theta)\,|\psi_{edge}(\theta_0)\rangle$, where θ_0 and $\theta_0 + \delta\theta$ define the type of polarization of the initial and final topological edge states.

To experimentally confirm such pseudo-spin conversion, we have fabricated samples where the domain wall in the PSH design with shrunken geometry on top gradually changes to the VH interface and then back to the PSH domain wall but with shrunken geometry on the bottom (rotated by π). The starting (1) and ending (3) regions of the resulting structure are known to support forward edge states that are spin-up [left-handed circular polarized (LCP) in far field] and spin-down [right-handed circular polarized (RCP) in far field], respectively, while the intermediate region (2) supports nonradiative VH edge states ($Q \to \infty$). As a whole, the structure is expected to operate as a pseudo-spin converter (a switch). In agreement with our predictions, our experiments in Fig. 4 show that LCP light incident on the PHS region (1) excites the pseudo-spin-up $|\uparrow\rangle$ edge mode propagating toward the right, which then darkens and disappears from the far field in the VH region (2) due to its conversion to a K-valley polarized $|+\rangle$ edge state, and lastly reappears in the inverted PSH region (3) as spin-down–polarized $|\downarrow\rangle$ edge state. Polarization resolved far-field measurements along the varying domain wall, shown in Fig. 4 (B to D), confirm that the edge mode gradually changes its polarization from LCP in region (1) to RCP in region (3). In the pseudo-spin subspace, the structure realizes an $\hat{X}_{spin} = \hat{s}_x$ gate operation. Similarly, a transition between two topologically distinct VH phases via intermediate PSH structure yields the valley-flip gate operation $\hat{X}_{valley} = \hat{\sigma}_x$. Because the proposed structures are reciprocal, a reversal of propagation direction reverses the operations, i.e., it flips spin and valley from the opposite initial state. However, because of the pseudo-spin locked character of the boundary modes, such operations are unidirectional, which is a unique functionality stemming from the topological nature of the system.

Geometrical phase and Aharonov-Bohm effect for topological edge modes

The described unitary transformations have another interesting consequence arising in the case of the evolution of heterogeneous edge states along the adiabatically varying interfaces. The edge states acquire a geometric (Berry-Pancharatnam type) phase (*61*, *62*) due to rotation along a path defined by the unitary transformation $\hat{U}[\delta\theta(x)]$ in the symmetry-engineered synthetic Hilbert space. Considering a cyclic evolution, e.g., $|\uparrow\rangle \to |+\rangle \to |\downarrow\rangle \to |-\rangle \to |\uparrow\rangle$, even a simple analysis based on the polarization state of the far-field radiation, and the respective evolution of the polarization state vector over the Poincaré sphere, yields the Pancharatnam phase of $\phi_{PB} \equiv \frac{\Omega}{2} = \pi$, where Ω is the solid angle enclosed by the evolution path on the Poincaré sphere. The continuity of the electromagnetic field of the modes requires that the same geometrical phase is acquired by the state as a whole $|\uparrow\rangle \to e^{ik_{\parallel}\Delta x}e^{i\pi}|\uparrow\rangle$ (including in the near field), where the first-phase factor accounts for the trivial dynamic phase accumulated after the wave travels the distance Δx along the domain wall and $k_{\parallel}$ is the edge wave number. Our first-principles simulations indeed confirm that the near field of the edge states acquires the same $\phi_{PB} = \pi$ geometric phase.

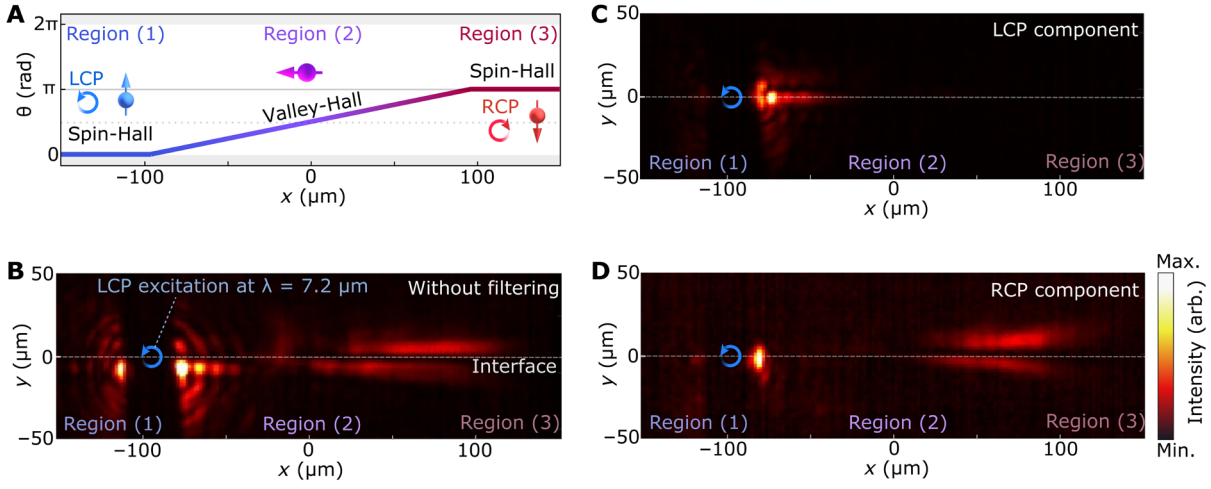

Fig. 4. Pseudo-spin conversion of topological boundary modes. (**A**) Parameter θ as a function of the x-coordinate along the adiabatically varying heterogeneous topological domain wall. (**B**) Real-space image of topological boundary modes with LCP excitation at θ = 0° without filtering. (**C**) LCP and (**D**) RCP components of the far field of the edge modes. The blue arrows in the real-space images present the position of LCP excitation with the spot size ~20 μm at 7.2 μm.

From this observation, we can expect that such geometric phase characterizes the transition regardless of the closed character of the loop. Our analytical model and numerical simulations confirm that a $\phi_{PB} = \pi$ phase shift arises every time we pass the $m_{s/v} = 0$ region. As an example, one-half of the cyclic evolution $|\downarrow\rangle \rightarrow |+\rangle \rightarrow |\uparrow\rangle$ in the spin-flipping switch described above must yield the state $e^{i\frac{\pi}{2}} |\uparrow\rangle$ (up to an irrelevant dynamic phase). Supplementary Materials, section A, provides a detailed analytical description of the geometrical phase due to the evolution of edge states on the full pseudo-spin–valley Bloch sphere. In such effective pseudo-spin–valley description the geometric phase can be given a different interpretation in terms of the flux of the synthetic gauge field generated by a monopole associated with the presence of the Dirac points at the Γ point in the momentum space (or K and K′ points in the unfolded Brillouin zone picture).

Although the translational symmetry along the interface is broken by the local character of the transformation $\hat{U}(x)$, its adiabatic character ensures that $k_{\parallel}$ is still a good "quantum number," (mixing with the backward solution is negligible). This condition is evidenced by the reflectionless propagation of the edge states through the adiabatic transition region with Δx of 80 unit cells (Fig. 4), while reflections do arise when the transition region is too short (e.g., just a few unit cells). The dependence of the edge transmission on the adiabaticity of the $\hat{U}(x)$ transformation is presented in Supplementary Materials, section E.

To experimentally confirm the accumulation of geometrical phase due to the adiabatic evolution, we carried out Young's type interferometry with two closely adjacent structures containing one domain wall each (see Fig. 5), only one of which realizes a flipping of spin state ($\Delta\theta = \pi$). Hence, this experiment is the direct analog of the Aharonov-Bohm effect (*63*) for these hybrid topological modes, which allows us to test the effect of synthetic gauge field flux and the geometrical phase it produces. Each domain wall in our structure effectively works as a slit, which couples ("transmits") a specific spin state ($|\uparrow\rangle$ or $|\downarrow\rangle$) into the structure. When the linearly polarized incident light is incident on one end of structure (input) with two different types of domain walls (labeled as 1 and 2), it excites two—spin-up and spin-down—edge states, respectively $\psi_{in} = |\uparrow\rangle_1 \otimes |\downarrow\rangle_2$ in the adjacent structures. As the modes propagate, the pseudo-spin of the second mode flips and acquires the geometrical phase $\pi/2$ at the other end of the structure (output), $\psi_{out} = |\uparrow\rangle_1 \otimes e^{i\frac{\pi}{2}} |\uparrow\rangle_2$ (up to an equal and thus irrelevant dynamic phase). By collimation light from the output region and imaging of the back focal plane yields an interference fringe pattern in the direction perpendicular to the domain walls, which should showcase the accumulation of the geometric phase. (Note that the detailed profile of fringe patterns as a whole is also defined by the far-field diffraction pattern of the individual domain walls.)

The interference allows us to directly observe the effect of the geometric phase on the superposition of far fields of the two edge states. Comparison of the interference patterns for the scenario without adiabatic evolution (Fig. 5A), which is used as a reference, with that corresponding to the edge state experiencing a spin flip (Fig. 5B) showcases a shift of the interference pattern by a quarter of the fringe pattern period (Fig. 5C), confirming the $\pi/2$ geometrical phase. For completeness, we also carried out an additional reference experiments with the second edge mode undergoing an adiabatic evolution but returning to its original pseudo-spin without flipping

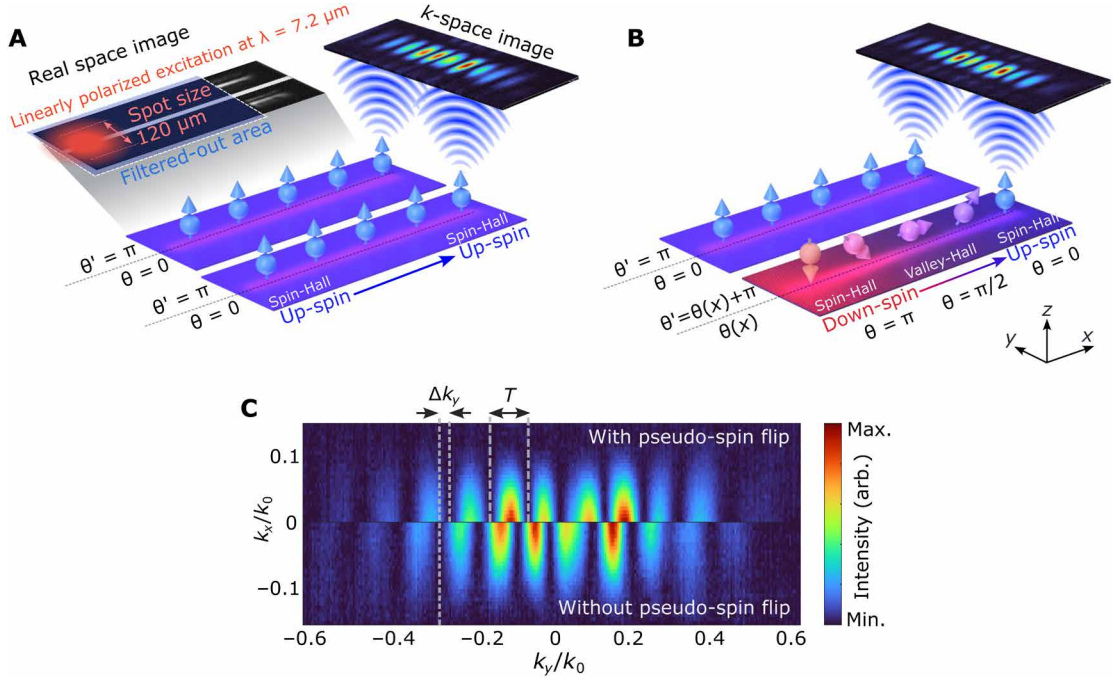

Fig. 5. Aharonov-Bohm effect for topological boundary modes. (**A** and **B**) Schematics and observed real-space and k-space images for interference patterns retrieved by the far-field diffraction patterns from two domain walls. (A) Two identical PSH domain walls, (B) a PSH domain wall, and a PSH-VH domain wall with adiabatic evolution $|\downarrow\rangle \rightarrow |+\rangle \rightarrow |\uparrow\rangle$. (**C**) Comparison between the two interference fringe patterns. Top: PSH domain wall and PSH-VH domain wall with adiabatic evolution $|\downarrow\rangle \rightarrow |+\rangle \rightarrow |\uparrow\rangle$. Bottom: Two identical PSH domain walls. *T* is the periodicity of interference patterns, and Δk_y is the interference pattern shift.

such that $|\uparrow\rangle \rightarrow |+\rangle \rightarrow |\uparrow\rangle$ (see Supplementary Materials, section G, and fig. S9). As expected, in such a scenario no shift of the interference pattern was observed, because the geometric phase accumulate in the first half of the evolution "unwinds" during its second half (see Supplementary Materials, section G, and fig. S10).

DISCUSSION

In this work, we demonstrated that synthetic gauge fields generated by combined spin and valley potentials in topological photonic crystals enable a class of heterogeneous topological boundary modes with controlled degree of pseudo-spin and valley polarizations, which allows precise tuning of the radiative properties of the topological boundary modes. Smooth variations of the gauge potentials along the domain walls supporting such heterogeneous boundary modes allows the implementation of topological one-way converters of polarization from spin to valley and vice versa, as well as reflectionless flipping of either spin of valley components, thus realizing unidirectional X-type quantum gates for either type of polarization. In turn, the adiabatic evolution of the edge states on the combined spin-valley Bloch sphere is accompanied by a geometric phase accumulation, which gave rise to the analog of an Aharonov-Bohm effect revealed in an experimentally Young's interference experiment. The versatile manipulation of pseudo-spins and phases of the edge states makes the heterogeneous topological photonic systems introduced here a promising platform for the implementation of quantum gates based on synthetic photonic DoFs. Moving toward experiments with quantum states of light, generated either externally or on chip, will be an interesting direction to pursue to unveil the potential of synthetic pseudo-spins and gauge fields for quantum applications.

MATERIALS AND METHODS

Sample fabrication

The fabrication of samples included patterning of silicon-on-sapphire substrates (1 μm of silicon and 500 μm of sapphire) via electron-beam lithography (EBL) and inductively coupled plasma (ICP) etching. A 300-nm-thick film of electron-beam resist ZEP520A7 followed by 50-nm-thick film of anticharging agent DisCharge H2Ox2 was spin-coated onto the substrate. The metasurface pattern was written into resist with EBL system Elionix ELS-G100 using 1-nA current, after which the anticharging agent was removed by rinsing the sample with deionized water and development of the resist was carried out in n-amyl acetate at 0°C for 1 min. Next, the pattern was etched through the mask of developed resist via ICP Oxford PlasmaPro System for the full depth with a recipe for anisotropic etching based on C_4F_8/SF_6 gases. The residue of unexposed resist was removed by immersing the sample in *N*-methyl-2-pyrrolidone solution heated to 60°C.

Experimental setup

To perform optical characterization of fabricated structures, we used a mid-infrared–operating custom-built setup equipped with a quantum cascade laser (QCL) Daylight MIRcat-1400 and a microbolometer camera INO MicroXcam-384-i. The scheme of the experimental setup is presented in Suppementary Materials, section I. The setup was designed for both real-space and Fourier-space imaging of a sample in reflection geometry at fixed wavelengths of QCL within the spectral range from 6.6 to 7.6 μm with a 5-nm fine step. The QCL beam was collimated, directed through a 50/50 CaF_2 beam splitter and focused on the sample surface by a refractive objective. We used a 0.56–numerical aperture Thorlabs Black Diamond molded aspheric lens (Thorlabs C028TME-F) as an objective, and excitation spot size was 20 μm. The collection path consisted of a set of two CaF_2 lenses with $f = 20$ cm. The position of the second lens determined what plane is imaged onto the camera's sensor: real-space or Fourier. Direct real-space imaging configuration of setup was used for visualization of topological boundary modes of fabricated photonic crystals, while interference patterns from edge states and band diagrams were extracted from Fourier-space configuration of the setup.

Experimental probing of band structures

For obtaining band structures of fabricated photonic crystals (Supplementary Materials, section G), we used Fourier-space imaging configuration of the experimental setup. Fourier-space imaging was implemented by so-called back focal plane imaging technique. Because the back focal plane of objective contains angular distribution of collected radiation, which is related to its momentum, the image of this plane recorded at a fixed wavelength represents in-plane momentum pattern or iso-frequency contour of fabricated structure. In the experimental setup, the back focal plane of operated objective was imaged on the camera's sensor in 4f configuration. By acquiring iso-frequency contours along with sequential tuning of the wavelength of the QCL, we reconstructed band diagrams from bulk and interface areas of fabricated photonic crystals.

Visualization of topological boundary modes

For direct imaging of localization and propagation of boundary modes along the topological interfaces, we used real-space configuration of the experimental setup with excitation by circularly polarized light focused on the domain wall of fabricated structures. For circularly polarized light excitation of edge modes, a tunable quarter-wave plate Alphalas PO-TWP-L4-25-IR was placed into the incident beam path right after the exit port of the QCL. Excitation of edge modes was performed around the mid-gap of fabricated structures at wavelength 7.20 μm. In experiments on topological one-way pseudo-spin switches, we implemented filtering of LCP and RCP components of the collected light by placing before the camera's sensor an additional quarter-wave plate paired with a BaF_2 holographic wire grid polarizer (Thorlabs WP25H-B). While the quarter-wave plate in collection path converted LCP and RCP light to linearly polarized light with orthogonal polarization angles, corresponding LCP and RCP components were filtered out by rotating the following polarizer by 90°.

Interferometry experiments

For interference experiments, the incident beam was expanded to 120 μm to cover a section of sample with two domain walls from two adjacent photonic crystals. It has been done by placing an additional CaF_2 lens with $f = 20$ cm in the excitation beam path before the beam splitter. Two edge states of adjacent structures were simultaneously excited with linearly polarized light with a wavelength 7.20 μm. Spatial filtering was implemented in the collection optical path to filter out the incident beam and keep the signal only from the region of structure where boundary modes of the structure with spin evolution experienced the spin flip and acquired

additional geometric phase. Because the real-space image of two propagating boundary modes in our experiments works as a plane with slits in Young's interference experiment, the interference pattern appears on Fourier plane, and it can be extracted from the back focal plane of operated objective. We used the Fourier-space imaging configuration of the experimental setup to record interference patterns for the same spatial positions of pairs of domain walls with various scenarios of spin evolution. By measuring the relative shift of interference fringe pattern for cases with and without spin flip, we were able to determine the presence of acquired additional geometric phase.

Supplementary Materials

This PDF file includes:

Sections A to I
Figs. S1 to S13

REFERENCES AND NOTES

1. M. Z. Hasan, C. L. Kane, Colloquium: Topological insulators. *Rev. Mod. Phys.* **82**, 3045–3067 (2010).
2. X. L. Qi, S. C. Zhang, Topological insulators and superconductors. *Rev. Mod. Phys.* **83**, 1057–1110 (2011).
3. X. Zhang, M. Xiao, Y. Cheng, M. H. Lu, J. Christensen, Topological sound. *Commun. Phys.* **1**, 97 (2018).
4. X. Zhang, F. Zangeneh-Nejad, Z. G. Chen, M. H. Lu, J. Christensen, A second wave of topological phenomena in photonics and acoustics. *Nature* **618**, 687–697 (2023).
5. S. D. Huber, Topological mechanics. *Nat. Phys.* **12**, 621–623 (2016).
6. L. Lu, J. D. Joannopoulos, M. Soljačić, Topological photonics. *Nat. Photonics* **8**, 821–829 (2014).
7. T. Ozawa, H. M. Price, A. Amo, N. Goldman, M. Hafezi, L. Lu, M. C. Rechtsman, D. Schuster, J. Simon, O. Zilberberg, I. Carusotto, Topological photonics. *Rev. Mod. Phys.* **91**, 015006 (2019).
8. H. Price, Y. Chong, A. Khanikaev, H. Schomerus, L. J. Maczewsky, M. Kremer, M. Heinrich, A. Szameit, O. Zilberberg, Y. Yang, Roadmap on topological photonics. *J. Phys. Photonics* **4**, 032501 (2022).
9. S. Raghu, F. D. M. Haldane, Analogs of quantum-Hall-effect edge states in photonic crystals. *Phys. Rev. A* **78**, 033834 (2008).
10. Z. Wang, Y. Chong, J. D. Joannopoulos, M. Soljačić, Observation of unidirectional backscattering-immune topological electromagnetic states. *Nature* **461**, 772–775 (2009).
11. M. Hafezi, E. A. Demler, M. D. Lukin, J. M. Taylor, Robust optical delay lines with topological protection. *Nat. Phys.* **7**, 907–912 (2011).
12. M. C. Rechtsman, J. M. Zeuner, Y. Plotnik, Y. Lumer, D. Podolsky, F. Dreisow, S. Nolte, M. Segev, A. Szameit, Photonic Floquet topological insulators. *Nature* **496**, 196–200 (2013).
13. A. B. Khanikaev, S. H. Mousavi, W. K. Tse, M. Kargarian, A. H. MacDonald, G. Shvets, Photonic topological insulators. *Nat. Mater.* **12**, 233–239 (2013).
14. L. Wu, X. Hu, Scheme for achieving a topological photonic crystal by using dielectric material. *Phys. Rev. Lett.* **114**, 223901 (2015).
15. T. Ma, G. Shvets, All-Si valley-Hall photonic topological insulator. *New J. Phys.* **18**, 025012 (2016).
16. F. Gao, H. Xue, Z. Yang, K. Lai, Y. Yu, X. Lin, Y. Chong, G. Shvets, B. Zhang, Topologically protected refraction of robust kink states in valley photonic crystals. *Nat. Phys.* **14**, 140–144 (2018).
17. H. Xue, Y. Yang, B. Zhang, Topological valley photonics: Physics and device applications. *Adv. Photonics Res.* **2**, 2100013 (2021).
18. C. A. Rosiek, G. Arregui, A. Vladimirova, M. Albrechtsen, B. V. Lahijani, R. E. Christiansen, S. Stobbe, Observation of strong backscattering in valley-Hall photonic topological interface modes. *Nat. Photonics* **17**, 386–392 (2023).
19. G. Harari, M. A. Bandres, Y. Lumer, M. C. Rechtsman, Y. D. Chong, M. Khajavikhan, D. N. Christodoulides, M. Segev, Topological insulator laser: Theory. *Science* **359**, aar4003 (2018).
20. L. Yang, G. Li, X. Gao, L. Lu, Topological-cavity surface-emitting laser. *Nat. Photonics* **16**, 279–283 (2022).
21. Y. Gong, S. Wong, A. J. Bennett, D. L. Huffaker, S. S. Oh, Topological insulator laser using valley-hall photonic Crystals. *ACS Photonics* **7**, 2089–2097 (2020).
22. B. Bahari, A. Ndao, F. Vallini, A. E. Amili, Y. Fainman, B. Kanté, Nonreciprocal lasing in topological cavities of arbitrary geometries. *Science* **358**, 636–640 (2017).
23. M. Hwang, H. Kim, J. Kim, B. Yang, Y. Kivshar, H. Park, Vortex nanolaser based on a photonic disclination cavity. *Nat. Photonics* **18**, 286–293 (2024).
24. D. Smirnova, D. Leykam, Y. Chong, Y. Kivshar, Nonlinear topological photonics. *Appl. Phys. Rev.* **7**, 021306 (2020).
25. M. S. Kirsch, Y. Zhang, M. Kremer, L. J. Maczewsky, S. K. Ivanov, Y. V. Kartashov, L. Torner, D. Bauer, A. Szameit, M. Heinrich, Nonlinear second-order photonic topological insulators. *Nat. Phys.* **17**, 995–1000 (2021).
26. L. J. Maczewsky, M. Heinrich, M. Kremer, S. K. Ivanov, M. Ehrhardt, F. Martinez, Y. V. Kartashov, V. V. Konotop, L. Torner, D. Bauer, A. Szameit, Nonlinearity-induced photonic topological insulator. *Science* **370**, 701–704 (2020).
27. A. V. Nalitov, D. D. Solnyshkov, G. Malpuech, PolaritonZTopological insulator. *Phys. Rev. Lett.* **114**, 116401 (2015).
28. T. Jacqmin, I. Carusotto, I. Sagnes, M. Abbarchi, D. D. Solnyshkov, G. Malpuech, E. Galopin, A. Lemaître, J. Bloch, A. Amo, Direct observation of Dirac cones and a flatband in a honeycomb lattice for polaritons. *Phys. Rev. Lett.* **112**, 116402 (2014).
29. T. Karzig, C. E. Bardyn, N. H. Lindner, G. Refael, Topological polaritons. *Phys Rev X* **5**, 031001 (2015).
30. S. Guddala, Y. Kawaguchi, F. Komissarenko, S. Kiriushechkina, A. Vakulenko, K. Chen, A. Alù, V. M. Menon, A. B. Khanikaev, All-optical nonreciprocity due to valley polarization pumping in transition metal dichalcogenides. *Nat. Commun.* **12**, 3746 (2021).
31. S. Guddala, F. Komissarenko, S. Kiriushechkina, A. Vakulenko, M. Li, V. M. Menon, A. Alù, A. B. Khanikaev, Topological phonon-polariton funneling in midinfrared metasurfaces. *Science* **374**, 225–227 (2021).
32. S. Mittal, E. A. Goldschmidt, M. Hafezi, A topological source of quantum light. *Nature* **561**, 502–506 (2018).
33. S. Barik, A. Karasahin, C. Flower, T. Cai, H. Miyake, W. DeGottardi, M. Hafezi, E. Waks, A topological quantum optics interface. *Science* **359**, 666–668 (2018).
34. M. Wang, C. Doyle, B. Bell, M. J. Collins, E. Magi, B. J. Eggleton, M. Segev, A. Blanco-Redondo, Topologically protected entangled photonic states. *Nanophotonics* **8**, 1327–1335 (2019).
35. A. Blanco-Redondo, B. Bell, D. Oren, B. J. Eggleton, M. Segev, Topological protection of biphoton states. *Science* **362**, 568–571 (2018).
36. Q. Yan, X. Hu, Y. Fu, C. Lu, C. Fan, Q. Liu, X. Feng, Q. Sun, Q. Gong, Quantum Topological Photonics. *Adv. Opt. Mater.* **9**, 2001739 (2021).
37. S. Kiriushechkina, A. Vakulenko, D. Smirnova, S. Guddala, Y. Kawaguchi, F. Komissarenko, M. Allen, J. Allen, A. B. Khanikaev, Spin-dependent properties of optical modes guided by adiabatic trapping potentials in photonic Dirac metasurfaces. *Nat. Nanotechnol.* **18**, 875–881 (2023).
38. G. Moody, V. J. Sorger, D. J. Blumenthal, P. W. Juodawlkis, W. Loh, C. Sorace-Agaskar, A. E. Jones, K. C. Balram, J. C. F. Matthews, A. Laing, M. Davanco, L. Chang, J. E. Bowers, N. Quack, C. Galland, I. Aharonovich, M. A. Wolff, C. Schuck, N. Sinclair, M. Lončar, T. Komljenovic, D. Weld, S. Mookherjea, S. Buckley, M. Radulaski, S. Reitzenstein, B. Pingault, B. Machielse, D. Mukhopadhyay, A. Akimov, A. Zheltikov, G. S. Agarwal, K. Srinivasan, J. Lu, H. X. Tang, W. Jiang, T. P. McKenna, A. H. Safavi-Naeini, S. Steinhauer, A. W. Elshaari, V. Zwiller, P. S. Davids, N. Martinez, M. Gehl, J. Chiaverini, K. K. Mehta, J. Romero, N. B. Lingaraju, A. M. Weiner, D. Peace, R. Cernansky, M. Lobino, E. Diamanti, L. T. Vidarte, R. M. Camacho, 2022 Roadmap on intregrated quantum photonics. *J. Phys. Photonics* **4**, 012501 (2022).
39. X.-T. He, E.-T. Liang, J.-J. Yuan, H.-Y. Qiu, X.-D. Chen, F.-L. Zhao, J.-W. Dong, A silicon-on-insulator slab for topological valley transport. *Nat. Commun.* **10**, 872 (2019).
40. M. I. Shalaev, W. Walasik, A. Tsukernik, Y. Xu, N. M. Litchinitser, Robust topologically protected transport in photonic crystals at telecommunication wavelengths. *Nat. Nanotechnol.* **14**, 31–34 (2019).
41. Y. Zeng, U. Chattopadhyay, B. Zhu, B. Qiang, J. Li, Y. Jin, L. Li, A. G. Davies, E. H. Linfield, B. Zhang, Y. Chong, Q. Wang, Electrically pumped topological laser with valley edge modes. *Nature* **578**, 246–250 (2020).
42. S. Barik, H. Miyake, W. Degottardi, E. Waks, M. Hafezi, Two-dimensionally confined topological edge states in photonic crystals. *New J. Phys.* **18**, 113013 (2016).
43. N. Parappurath, F. Alpeggiani, L. Kuipers, E. Verhagen, Direct observation of topological edge states in silicon photonic crystals: Spin, dispersion, and chiral routing. *Sci. Adv.* **6**, aaw4137 (2020).
44. M. A. Gorlach, X. Ni, D. A. Smirnova, D. Korobkin, D. Zhirihin, A. P. Slobozhanyuk, P. A. Belov, A. Alù, A. B. Khanikaev, Far-field probing of leaky topological states in all-dielectric metasurfaces. *Nat. Commun.* **9**, 909 (2018).
45. Y. Plotnik, M. C. Rechtsman, D. Song, M. Heinrich, J. M. Zeuner, S. Nolte, Y. Lumer, N. Malkova, J. Xu, A. Szameit, Z. Chen, M. Segev, Observation of unconventional edge states in 'photonic graphene'. *Nat. Mater.* **13**, 57–62 (2014).
46. J. Mei, Z. Chen, Y. Wu, Pseudo-time-reversal symmetry and topological edge states in two-dimensional acoustic crystals. *Sci. Rep.* **6**, 32752 (2016).
47. X. Ni, D. Purtseladze, D. A. Smirnova, A. Slobozhanyuk, A. Alù, A. B. Khanikaev, Spin- and valley-polarized one-way Klein tunneling in photonic topological insulators. *Sci. Adv.* **4**, aap8802 (2018).
48. Y. Kang, X. Ni, X. Cheng, A. B. Khanikaev, A. Z. Genack, Pseudo-spin–valley coupled edge states in a photonic topological insulator. *Nat. Commun.* **9**, 3029 (2018).

49. J. Ma, X. Xi, Y. Li, X. Sun, Nanomechanical topological insulators with an auxiliary orbital degree of freedom. *Nat. Nanotechnol.* **16**, 576–583 (2021).
50. G. Ma, M. Xiao, C. T. Chan, Topological phases in acoustic and mechanical systems. *Nat. Rev. Phys.* **1**, 281–294 (2019).
51. J. W. Dong, X. D. Chen, H. Zhu, Y. Wang, X. Zhang, Valley photonic crystals for control of spin and topology. *Nat. Mater.* **16**, 298–302 (2017).
52. J. Noh, T. Schuster, T. Iadecola, S. Huang, M. Wang, K. P. Chen, C. Chamon, M. C. Rechtsman, Braiding photonic topological zero modes. *Nat. Phys.* **16**, 989–993 (2020).
53. S. Han, Y. Chua, Y. Zeng, B. Zhu, C. Wang, B. Qiang, Y. Jin, Q. Wang, L. Li, A. G. Davies, E. H. Linfield, Y. Chong, B. Zhang, Q. J. Wang, Photonic Majorana quantum cascade laser with polarization-winding emission. *Nat. Commun.* **14**, 707 (2023).
54. X. Gao, L. Yang, H. Lin, L. Zhang, J. Li, F. Bo, Z. Wang, L. Lu, Dirac-vortex topological cavities. *Nat. Nanotechnol.* **15**, 1012–1018 (2020).
55. J. Košata, O. Zilberberg, Second-order topological modes in two-dimensional continuous media. *Phys. Rev. Res.* **3**, L032029 (2021).
56. G. H. Wannier, Dynamics of band electrons in electric and magnetic fields. *Rev. Mod. Phys.* **34**, 645–655 (1962).
57. G. H. Wannier, The structure of electronic excitation levels in insulating crystals. *Phys. Rev.* **52**, 191–197 (1937).
58. B. Bradlyn, L. Elcoro, J. Cano, M. G. Vergniory, Z. Wang, C. Felser, M. I. Aroyo, B. A. Bernevig, Topological quantum chemistry. *Nature* **547**, 298–305 (2017).
59. W. A. Benalcazar, B. A. Bernevig, T. L. Hughes, Electric multipole moments, topological multipole moment pumping, and chiral hinge states in crystalline insulators. *Phys. Rev. B* **96**, 245115 (2017).
60. A. Vakulenko, S. Kiriushechkina, D. Smirnova, S. Guddala, F. Komissarenko, A. Alù, M. Allen, J. Allen, A. B. Khanikaev, Adiabatic topological photonic interfaces. *Nat. Commun.* **14**, 4629 (2023).
61. M. Berry, Quantal phase factors accompanying adiabatic changes. *Proc. R. Soc. Lond. Ser. A Math. Phys. Sci.* **392**, 45–57 (1984).
62. S. Pancharatnam, Generalized theory of interference, and its applications. *Proc. Indian Acad. Sci. Sect. A* **44**, 247–262 (1956).
63. Y. Aharonov, D. Bohm, Significance of electromagnetic potentials in the quantum theory. *Phys. Rev.* **115**, 485–491 (1959).

Acknowledgments: The fabrication of samples was performed at the Nanofabrication Facility at the Advanced Science Research Center at The Graduate Center of the City University of New York. **Funding:** A.B.K. and A.A. acknowledge support from the Simons Foundation and the Office of Naval Research. A.B.K. acknowledges support by the NSF awards no. 1809915 and no. 2328993. D.S. acknowledges support from the Australian Research Council (FT230100058). **Author contributions:** Conceptualization: Y.K., D.S., A.A., and A.B.K. Methodology: Y.K., D.S., A.A., and A.B.K. Investigation: Y.K., F.K., S.K., and A.V. Formal analysis: Y.K., D.S., and M.L. Software: Y.K., D.S., and A.B.K. Validation: Y.K., D.S., and A.B.K. Data curation: Y.K. Visualization: Y.K., D.S., M.L., and A.B.K. Resources: S.K. and A.B.K. Supervision: Y.K., A.A., and A.B.K. Project administration: Y.K., A.A., and A.B.K. Writing—original draft: Y.K., D.S., F.K., and A.B.K. Writing—review and editing: Y.K., F.K., M.L., A.A., and A.B.K. **Competing interests:** The authors declare that they have no competing interests. **Data and materials availability:** All data needed to evaluate the conclusions in the paper are present in the paper and/or the Supplementary Materials.

Submitted 18 December 2023
Accepted 12 March 2024
Published 12 April 2024
10.1126/sciadv.adn6095